How accurately can subject-specific finite element models predict strains and strength of human femora? Investigation using full-field measurements

Grassi, Lorenzo; Väänänen, Sami P.; Ristinmaa, Matti; Jurvelin, Jukka S.; Isaksson, Hanna

Published in:
Journal of Biomechanics

DOI:
10.1016/j.jbiomech.2016.02.032

2016

www.elsevier.com/locate/jbiomech

How accurately can subject-specific finite element models predict strains and strength of human femora? Investigation using full-field measurements

Lorenzo Grassi, Sami P. Väänänen, Matti Ristinmaa, Jukka S. Jurvelin, Hanna Isaksson

PII: S0021-9290(16)30186-5
DOI: http://dx.doi.org/10.1016/j.jbiomech.2016.02.032
Reference: BM7597

To appear in: *Journal of Biomechanics*

Received date: 24 December 2015
Revised date: 11 February 2016
Accepted date: 12 February 2016

Cite this article as: Lorenzo Grassi, Sami P. Väänänen, Matti Ristinmaa, Jukka S Jurvelin and Hanna Isaksson, How accurately can subject-specific finite elemer models predict strains and strength of human femora? Investigation using full field measurements, *Journal of Biomechanics* http://dx.doi.org/10.1016/j.jbiomech.2016.02.032

Lorenzo Grassi[1], Sami P. Väänänen[2], Matti Ristinmaa[3], Jukka S. Jurvelin[2,4], Hanna Isaksson[1]

[1] Department of Biomedical Engineering, Lund University, Sweden
[2] Department of Applied Physics, University of Eastern Finland, Finland
[3] Division of Solid Mechanics, Lund University, Sweden
[4] Diagnostic Imaging Center, Kuopio University Hospital, Finland

HOW ACCURATELY CAN SUBJECT-SPECIFIC FINITE ELEMENT MODELS PREDICT STRAINS AND STRENGTH OF HUMAN FEMORA? INVESTIGATION USING FULL-FIELD MEASUREMENTS.

SUBMITTED AS A

SHORT COMMUNICATION

CORRESPONDING AUTHOR:

Lorenzo Grassi

Department of Biomedical Engineering, Lund University

BMC D13, 221 84 Lund, Sweden

Email: lorenzo.grassi@bme.lth.se

Telephone:+46 46 222 06 55

ABSTRACT

Subject-specific finite element models have been proposed as a tool to improve fracture risk assessment in individuals. A thorough laboratory validation against experimental data is required before introducing such models in clinical practice. Results from digital image correlation can provide full-field strain distribution over the specimen surface during in vitro test, instead of at a few pre-defined locations as with strain gauges. The aim of this study was to validate finite element models of human femora against experimental data from three cadaver femora, both in terms of femoral strength and of the full-field strain distribution collected with digital image correlation. The results showed a high accuracy between predicted and measured principal strains (R^2=0.93, RMSE=10%, 1600 validated data points per specimen). Femoral strength was predicted using a rate dependent material model with specific strain limit values for yield and failure. This provided an accurate prediction (<2% error) for two out of three specimens. In the third specimen, an accidental change in the boundary conditions occurred during the experiment, which compromised the femoral strength validation. The achieved strain accuracy was comparable to that obtained in state-of-the-art studies which validated their prediction accuracy against 10-16 strain gauge measurements. Fracture force was accurately predicted, with the predicted failure location being very close to the experimental fracture rim. Despite the low sample size and the single loading condition tested, the present combined numerical-experimental method showed that finite element models can predict femoral strength by providing a thorough description of the local bone mechanical response.

KEYWORDS

Finite element, human femur, experimental validation, bone strength

INTRODUCTION

Fragility fractures due to osteoporosis are a huge problem in Western society (Burge et al., 2007). Pharmacological treatment can increase strength of osteoporotic bones and reduce fracture risk (Kanis et al., 2013) but should be targeted to individuals whose risk of fracture is highest (Lindsay et al., 2005).

Osteoporosis is diagnosed based on bone mineral density measured in the proximal femur or lumbar spine using Dual-Energy X-ray absorptiometry. By including epidemiological parameters, fracture risk is estimated (Cummings et al., 2006; Kanis et al., 2005). This method has a relatively poor accuracy (30% false negatives, (Järvinen et al., 2005; McCreadie and Goldstein, 2000)), and is ethnic-specific (Watts et al., 2009). Subject-specific finite element (FE) models from computed tomography (CT) scans can increase the prediction accuracy by providing a comprehensive description of the bone's mechanical response. Although the prediction accuracy is considerably high both for strains (R^2>0.95, (Schileo et al., 2008; Yosibash et al., 2007)) and femoral strength (standard error of estimation(SEE)<400 N, (Koivumäki et al., 2012)), FE models have not yet been introduced in clinical practice. This is due to several reasons including concerns about validation (Henninger et al., 2010; Viceconti et al., 2005). Typically, validation against ex-vivo measurements with strain-gauges is performed. This limits the data to ~10-15 measurements at pre-selected spots (Grassi and Isaksson, 2015). Optical methods like digital image correlation (DIC) (Gilchrist et al., 2013; Helgason et al., 2014; Op Den Buijs and Dragomir-Daescu, 2011) provide a more comprehensive validation benchmark. We recently collected DIC measurements at a physiological loading rate on three femora (Grassi et al., 2014), suited for reliable validation of FE models.

Therefore, the aim of the present study was to predict fracture load in human femora using subject-specific FE models. Validation was performed for strains calculated with FE against strains measured experimentally with DIC, and for femoral strength calculated with FE against the maximum force recorded experimentally.

MATERIAL AND METHODS

Three male cadaver human proximal femora were harvested fresh at Kuopio University Hospital, Finland (ethical permission 5783/2004/044/07). None of the donors had any reported musculoskeletal disorder. Height, weight, sex and age at death are reported in table 1. The specimens were CT scanned (Definition AS64, Siemens AG, 0.4x0.4x0.6 mm voxel size).

Mechanical testing

The three femora were mechanically tested to failure in a single-leg-stance configuration, and strains were measured using DIC. The experimental protocol was reported in detail in (Grassi et al., 2014). Briefly, the specimens were cleaned and resected 5.5 cm below the minor trochanter. The femoral shaft below the minor trochanter was embedded in epoxy and constrained. A stainless steel cap was applied on the femoral head to distribute the load and avoid local crushing. The gap between the cap and the femoral head was filled with epoxy. The anterior surface was prepared for DIC by applying a random black speckle pattern over a matt white background. Mechanical tests were performed in a single-leg-stance configuration, with the load applied on the femoral head parallel to the shaft axis. Specimens were loaded at 15 mm/s until macroscopic failure. DIC was performed on the acquired images (two Fastcam SA1.1, Photron, Inc., 3000 frames per second; VIC 3D v7, Correlated Solutions, Inc., 25 px subset, 5 px step, 100 Hz low-pass displacement filter), and the Green-Lagrange strains were retrieved at each frame (~10000 uniquely traceable points per specimen) (Grassi et al., 2014).

Finite element modelling

FE models were generated using a consolidated procedure (Grassi et al., 2013; Schileo et al., 2008). Femur geometry was semi-automatically segmented from CT (threshold, dilation/erosion, and manual correction, Seg3D2, University of Utah). The geometries were reverse-engineered (Rhinoceros 4.0, Robert McNeel & Associates, USA, and RhinoResurf, Resurf3d, China), and a second-order tetrahedral mesh (~140000 nodes,

~100000 elements, Hypermesh v13.0, Altair Engineering) was created. Elements in the epoxy pot were assigned an isotropic Young's modulus of 2.5GPa, (Technovit 4071, Heraeus Kulzer). Elements belonging to the femur were assigned Young's modulus based on the Hounsfield Unit (HU) values. CT images were reconstructed using a sharp convolution kernel (B60f). Each axial slice was filtered using a mean filter of 4x4 pixel size to compensate for the HU overestimation due to this kernel. Bonemat_V3 (Taddei et al., 2007) assigned inhomogeneous isotropic material properties to the elements, based on the HU values of the volume enclosed by each element. HU values were converted to equivalent radiological density (Model 3CT, Mindways Inc.), and the Young's modulus was derived using the relationships proposed by (Schileo et al., 2008). Poisson's ratio was set to 0.4 (Reilly and Burstein, 1975). The geometry of the epoxy pot was used to identify the experimental reference system (figure 1). The load was equally distributed among the 10 most superior surface nodes on the femoral head. FE simulations were solved using Abaqus (v6.12-4, Dassault Systèmes).

Strain prediction accuracy

Strain prediction accuracy was evaluated at a force of four times the body weight (BW). The predicted principal strains were compared to DIC measurements. A registration and data comparison method was adopted, based on a procedure that earlier provided good results for composite bones (Grassi et al., 2013). The DIC point cloud was registered over the FE model using an iterative closest point approach. For each surface element, the smallest sphere circumscribing it was calculated. All DIC data lying within the sphere were averaged, and the obtained value compared to the FE element strain. A robust regression analysis with bisquare weighting function of the major and minor principal strain magnitudes was performed to assess the accuracy. Bland-Altman plots (Bland and Altman, 1999) provided a visual interpretation of the agreement between predicted and measured principal strains.

Femoral strength prediction accuracy

The FE models implemented a rate-dependent material model, with different strain limit values for yield and failure (figure 2). Each element was assigned its specific initial

modulus (E_{elem}^{ref}) as described above. A strain rate correction factor: $SRCF_{elem} = (\dot{\varepsilon}_{elem}/\dot{\varepsilon}_{ref})^{0.006}$ was defined, where $\dot{\varepsilon}_{elem}$ is the absolute major principal strain rate, and $\dot{\varepsilon}_{ref}$ is the strain rate at which yield values and density-elasticity relationship were obtained (5000 με/s, (Bayraktar et al., 2004; Morgan et al., 2003)). The tangent modulus was defined as: $E_{elem}(SRCF) = SRCF_{elem} * E_{elem}^{ref}$.

Different limit strain values in tension (major principal strains) and compression (minor principal strains) were implemented for yield and failure. When element strain exceeded the yield strain limit (10400 με compression, 7300 με tension, (Bayraktar et al., 2004)), the modulus was reduced to 5.5% of the tangent modulus (Reilly et al., 1974), and the simulation continued. An element was considered failed when the ultimate strain limit was exceeded (21000 με compression, 26050 με tension (Reilly et al., 1974)).

The FE analysis was conducted by applying consecutive 0.05 mm increments, with the time increment tuned to 15 mm/s displacement rate. The specimen was considered failed when the first element failed, and the applied force taken as the predicted femoral strength. This value was compared to the maximum force recorded during the experiment. Relative error and SEE were reported. The predicted fracture onset location was qualitatively compared to the experimental fracture rim.

RESULTS

Strain prediction accuracy

For the three bones pooled (4826 data points), principal strains magnitudes were predicted with a determination coefficient (R^2) of 0.94. The regression slope was 0.96, and the intercept 133 με. The normalized root mean square error (NRMSE) was 9%. The predicted versus measured principal strains and the Bland-Altman plot are reported

in figure 3. When validating each bone individually (figure 3), R^2 was always >0.9, with slope and intercept close to 1 and 0, respectively.

Femoral strength prediction accuracy

Femoral strength was predicted with an error of -1.5% and +1.2% for bone #1 and #2, respectively (SEE=155 N, table 2). Femoral strength for the third specimen could not be validated because the cap slipped experimentally, which changed the prescribed boundary conditions. FE models predicted failure to initiate in compression on the medial aspect of the neck. The predicted fracture onset was <1 cm away from the experimental fracture line (figure 4).

DISCUSSION

This study aimed to assess the ability of subject-specific FE models to predict principal strains and femoral strength in human femora. This is, to our knowledge, the first study reporting a strain-fracture load FE validation against full-field strain measurements at physiologically relevant strain rates (maximum strain rate 0.032-0.053s^{-1}, (Grassi et al., 2014)).

Strains were predicted with a high accuracy (R^2=0.94, NRMSE=9%), comparable to the highest reported for human femora in analogous loading configurations (R^2=0.95-0.97, (Schileo et al., 2008; Yosibash et al., 2007)). The strain accuracy in those studies was obtained against ~10 measurements. In this study, ~1600 measurements covering the femur anterior surface (Grassi et al., 2014) were used. This corroborates the validity of our FE modelling approach, and represents one of the strengths of this study. The majority of the points laid within the confidence limits of the Bland-Altman plots, with no observable trends in the distribution (figure 3).

Rate-dependent material with strain limit values for yield and failure was implemented. Limit values were taken from literature (Bayraktar et al., 2004; Reilly and Burstein, 1974). SRCF was defined, similar to Schileo et al. (2014). However, they applied a constant SRCF to all elements. In our implementation, SRCF was calculated for each

element, and updated at every time increment, thus more realistically describing the rate dependency of bone.

Femoral strength was accurately predicted for the first two specimens (-1.5% and +1.2%). SEE was comparable to the best published results (Bessho et al., 2007; Koivumäki et al., 2012). The latter were obtained using some specimens to train the models and identify the optimal strain/stress limit values, and validating the predictions over the remaining specimens. Our approach is instead free from internal parameter calibration, and uses limit values from experiments investigating bone properties at the mesoscale level.

Fracture load was not validated for the third specimen, since the cap slipped during the experiment. As a result, specimen #3 exhibited a peculiar fracture pattern: the crack originated close to the rim of the cap and propagated vertically (Grassi et al., 2014).

Failure onset was predicted on the medial aspect of the neck, a region mainly in compression. The onsets were close to the experimental fracture rim (figure 4). The experimental images show the crack originating on the superolateral aspect of the neck (Grassi et al., 2014), which is predominantly loaded in tension. We hypothesize that macroscopic crack formation was a consequence of a compressive failure of the medial side of the neck, occurring fractions of milliseconds before the crack formation. A similar two-step failure mechanism has been reported for femora in side-fall (de Bakker et al., 2009). There, high-speed cameras placed on the medial and lateral aspect showed a two-step failure, where the first failure was in compression on the superolateral aspect. The macroscopic crack occurred immediately after on the contralateral side. An analogous mechanism, with medial and lateral side inverted due to the different loading direction, can very well occur in single-leg-stance. In our experiment, no video recordings of medial and lateral side was available, leaving the question about fracture onset unanswered. Future experiments investigating bone fracture should, whenever possible, use more cameras covering a broader area.

This study is limited by its small sample size, with three specimens tested. A second limitation regards specimen #3, whose fracture load could not be validated due to the

cap slippage. Nevertheless, the strain response for specimen #3 was analysed at 4BW, since slippage occurred later. Specimen #3 showed a very high strain accuracy (R^2=0.94, slope=0.99, figure 3), which corroborates the accuracy of the proposed FE modelling approach in predicting femoral mechanical behaviour. The single loading direction investigated is also limiting. Future works will aim at extending our combined experimental/numerical approach to a sideways fall configuration.

In summary, a simple subject-specific FE modelling technique, free from internal parameter calibration, accurately predicted the mechanical behaviour of human femora in a single-leg-stance configuration, both in terms of strain response and fracture load. These results support the translation of FE into clinical studies, where the predicted bone strength could complement epidemiological parameters in fracture risk estimation.

ACKNOWLEDGEMENTS

The authors wish to thank Aleksandra Turkiewicz for the help with the statistical analysis. The study was supported by the Swedish Research Council (2011-5064), Finnish Cultural Foundation and University of Eastern Finland (929711) strategic funding.

CONFLICT OF INTEREST STATEMENT

None of the authors had conflict of interest to declare.

REFERENCES

Bayraktar, H.H., Morgan, E.F., Niebur, G.L., Morris, G.E., Wong, E.K., Keaveny, T.M., 2004. Comparison of the elastic and yield properties of human femoral trabecular and cortical bone tissue. J. Biomech. 37, 27–35. doi:10.1016/S0021-9290(03)00257-4

Bessho, M., Ohnishi, I., Matsuyama, J., Matsumoto, T., Imai, K., Nakamura, K., 2007. Prediction of strength and strain of the proximal femur by a CT-based finite element method. J. Biomech. 40, 1745–53. doi:10.1016/j.jbiomech.2006.08.003

Bland, J.M., Altman, D.G., 1999. Measuring agreement in method comparison studies. Stat. Methods Med. Res. 8, 135–160. doi:10.1177/096228029900800204

Burge, R., Dawson-Hughes, B., Solomon, D.H., Wong, J.B., King, A., Tosteson, A., 2007. Incidence and economic burden of osteoporosis-related fractures in the United States, 2005-2025. J. Bone Miner. Res. 22, 465–75. doi:10.1359/jbmr.061113

Cummings, S.R., Cawthon, P.M., Ensrud, K.E., Cauley, J.A., Fink, H.A., Orwoll, E.S., 2006. BMD and risk of hip and nonvertebral fractures in older men: a prospective study and comparison with older women. J. Bone Miner. Res. 21, 1550–6. doi:10.1359/jbmr.060708

de Bakker, P.M., Manske, S.L., Ebacher, V., Oxland, T.R., Cripton, P.A., Guy, P., 2009. During sideways falls proximal femur fractures initiate in the superolateral cortex: evidence from high-speed video of simulated fractures. J. Biomech. 42, 1917–25. doi:10.1016/j.jbiomech.2009.05.001

Gilchrist, S., Guy, P., Cripton, P. a, 2013. Development of an inertia-driven model of sideways fall for detailed study of femur fracture mechanics. J. Biomech. Eng. 135, 121001. doi:10.1115/1.4025390

Grassi, L., Isaksson, H., 2015. Extracting accurate strain measurements in bone mechanics: a critical review of current methods. J. Mech. Behav. Biomed. Mater. 50, 43–54. doi:doi:10.1016/j.jmbbm.2015.06.006

Grassi, L., Väänänen, S.P., Amin Yavari, S., Jurvelin, J.S., Weinans, H., Ristinmaa, M., Zadpoor, A.A., Isaksson, H., 2014. Full-field Strain Measurement During Mechanical Testing of the Human Femur at Physiologically Relevant Strain Rates. J. Biomech. Eng. 136. doi:10.1115/1.4028415

Grassi, L., Väänänen, S.P., Amin Yavari, S., Weinans, H., Jurvelin, J.S., Zadpoor, A. a., Isaksson, H., 2013. Experimental Validation Of Finite Element Model For Proximal Composite Femur Using Optical Measurements. J. Mech. Behav. Biomed. Mater.

21, 86–94. doi:10.1016/j.jmbbm.2013.02.006

Helgason, B., S Gilchrist, Ariza, O., Chak, J.D., Zheng, G., Widmer, R.P., Ferguson, S.J., Guy, P., Cripton, P. a, 2014. Development of a balanced experimental-computational approach to understanding the mechanics of proximal femur fractures. Med. Eng. Phys. 36, 793–799. doi:10.1016/j.medengphy.2014.02.019

Henninger, H., Reese, S., Anderson, A., Weiss, J., 2010. Validation of computational models in biomechanics. Proc. … 224, 801–812.

Järvinen, T.L.N., Sievänen, H., Jokihaara, J., Einhorn, T.A., 2005. Revival of Bone Strength: The Bottom Line. J. Bone Miner. Res. 20, 717–720.

Kanis, J.A., Borgstrom, F., De Laet, C., Johansson, H., Johnell, O., Jonsson, B., Oden, A., Zethraeus, N., Pfleger, B., Khaltaev, N., 2005. Assessment of fracture risk. Osteoporos. Int. 16, 581–9. doi:10.1007/s00198-004-1780-5

Kanis, J.A., McCloskey, E. V, Johansson, H., Cooper, C., Rizzoli, R., Reginster, J.-Y., 2013. European guidance for the diagnosis and management of osteoporosis in postmenopausal women. Osteoporos. Int. 24, 23–57. doi:10.1007/s00198-012-2074-y

Koivumäki, J.E.M., Thevenot, J., Pulkkinen, P., Kuhn, V., Link, T.M., Eckstein, F., Jämsä, T., 2012. Ct-based finite element models can be used to estimate experimentally measured failure loads in the proximal femur. Bone 50, 824–829. doi:10.1016/j.bone.2012.01.012

Lindsay, R., Pack, S., Li, Z., 2005. Longitudinal progression of fracture prevalence through a population of postmenopausal women with osteoporosis. Osteoporos. Int. 16, 306–12. doi:10.1007/s00198-004-1691-5

McCreadie, B.R., Goldstein, S.A., 2000. Biomechanics of fracture: is bone mineral density sufficient to assess risk? J Bone Min. Res 15, 2305–2308.

Morgan, E.F., Bayraktar, H.H., Keaveny, T.M., 2003. Trabecular bone modulus-density relationships depend on anatomic site. J. Biomech. 36, 897–904.

Op Den Buijs, J., Dragomir-Daescu, D., 2011. Validated finite element models of the proximal femur using two-dimensional projected geometry and bone density. Comput. Methods Programs Biomed. 104, 168–74. doi:10.1016/j.cmpb.2010.11.008

Reilly, D., Burstein, A., 1974. The mechanical properties of cortical bone. J. Bone Jt. Surg. 56.

Reilly, D., Burstein, A., Frankel, V., 1974. The elastic modulus for bone. J. Biomech. 7, 271–275.

Reilly, D.T., Burstein, a H., 1975. The elastic and ultimate properties of compact bone

tissue. J. Biomech. 8, 393–405. doi:10.1016/0021-9290(75)90075-5

Schileo, E., Balistreri, L., Grassi, L., Cristofolini, L., Taddei, F., 2014. To what extent can linear finite element Models of Human femora predict failure under stance and fall loading configurations? J. Biomech. 47, 3531–3538. doi:10.1016/j.jbiomech.2014.08.024

Schileo, E., Dall'ara, E., Taddei, F., Malandrino, A., Schotkamp, T., Baleani, M., Viceconti, M., 2008. An accurate estimation of bone density improves the accuracy of subject-specific finite element models. J. Biomech. 41, 2483–2491.

Taddei, F., Schileo, E., Helgason, B., Cristofolini, L., Viceconti, M., 2007. The material mapping strategy influences the accuracy of CT-based finite element models of bones: an evaluation against experimental measurements. Med. Eng. Phys. 29, 973–9. doi:10.1016/j.medengphy.2006.10.014

Watts, N.B., Ettinger, B., LeBoff, M.S., 2009. FRAX facts. J. Bone Miner. Res. 24, 975–9. doi:10.1359/jbmr.090402

Viceconti, M., Olsen, S., Nolte, L.-P., Burton, K., 2005. Extracting clinically relevant data from finite element simulations. Clin. Biomech. (Bristol, Avon) 20, 451–4. doi:10.1016/j.clinbiomech.2005.01.010

Yosibash, Z., Trabelsi, N., Milgrom, C., 2007. Reliable simulations of the human proximal femur by high-order finite element analysis validated by experimental observations. J. Biomech. 40, 3688–99. doi:10.1016/j.jbiomech.2007.06.017

FIGURE LEGENDS

Figure 1: Overview of the study. Top left: the subject-specific FE models were built starting from the CT scan through a process of segmentation, reverse engineering, tetrahedral meshing, and material property mapping based on the calibrated CT values. The origin of the experimental reference system was set in a base corner of the epoxy pot, with x-axis and y-axis aligned to horizontal and vertical side, respectively. The load was applied along the negative y-direction on the femoral head. Bottom left: schematic of the experimental setup. The specimens were tested until fracture in a single leg stance position, and deformations measured using a 3D surface digital image correlation (Grassi et al., 2014). Right: the FE predictions were compared to the measured principal strains by registering the experimental point cloud over the FE model, and then averaging the experimental values within each element's volume of interest.

Figure 2: The material model implemented in the FE models to predict bone strength. The response was strain rate dependent, according to the defined strain rate correction factor (SRCF). The behaviour of one element for two different values of SRCF is shown in the stress strain diagram. Bone strength was predicted using threshold strain values for yield (ε_y) and failure (ε_f). Different thresholds were chosen for tension ("t" superscript) and compression ("c" superscript). The post-yield modulus was set to 5.5 % of the modulus in the elastic range, as extrapolated from the measurements reported in (Reilly et al., 1974).

Figure 3: Prediction accuracy for the principal strains for the three bones pooled (top) and for each bone separately (row 2-4). The applied force was 4 times the subjects' body weight. The robust linear regression analyses are shown on the left, and Bland-Altman plots on the right. The dotted lines represent the 95 % confidence interval.

Figure 4: Top: graphical comparison of the experimentally obtained fracture rim (black) with the fracture onset location predicted by the FE models (red). Middle: the experimentally measured major principal strains at 0.3 ms before a crack was detected in the DIC images are superimposed to the fracture rim and the predicted fracture onset. Bottom: the experimentally measured minor principal strains at 0.3 ms before a crack was detected in the DIC images are superimposed to the fracture rim and the predicted fracture onset.

TABLE LEGENDS

Table 1: Patient information (sex, age at death, height, weight, and leg side) for the three specimens used in this study.

Specimen ID	**Sex (M/F)**	**Age [years]**	**Height [cm]**	**Weight [kg]**	**Side (L/R)**
#1	M	22	186	106	L

#2	M	58	183	85	R
#3	M	58	183	112	L

Table 2: Bone strength of the three specimens used in this study as measured during the experiments (Grassi et al., 2014), and predicted using FE models.

	Bone #1	**Bone #2**
Experimental strength [N]	13383	7856
Predicted strength [N]	13184	7947
Difference [%]	– 1.5 %	+1.2 %

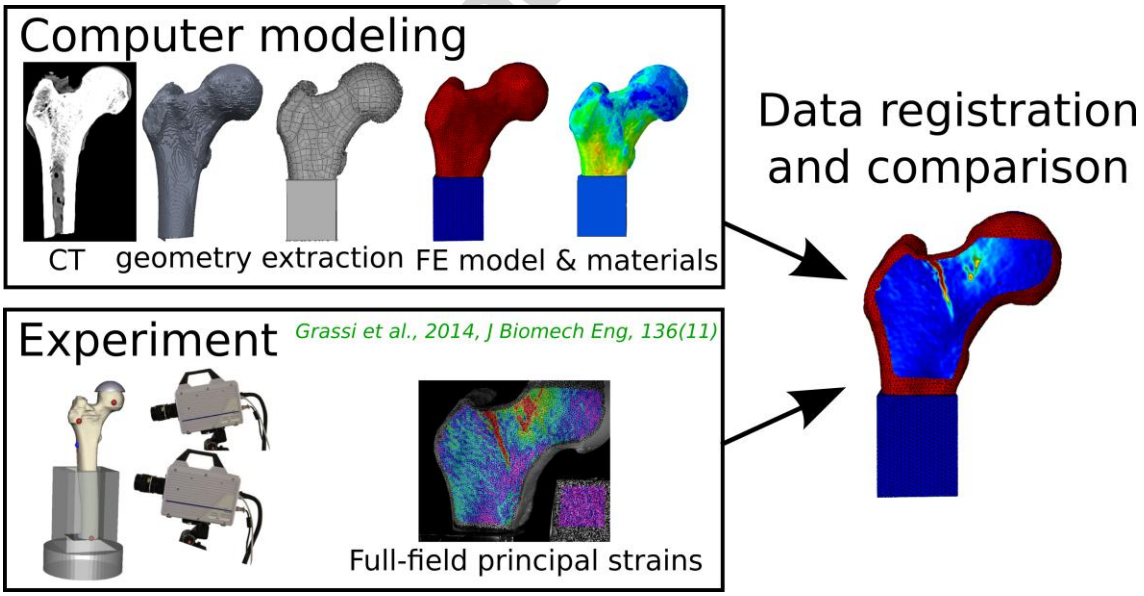

fig 1

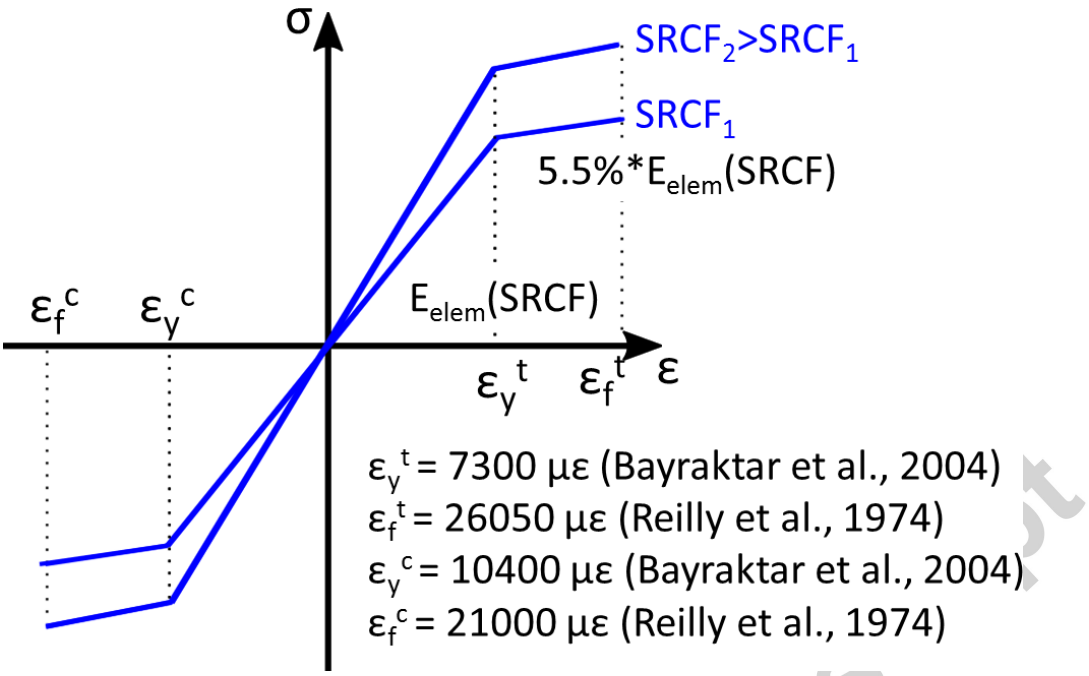

fig 2

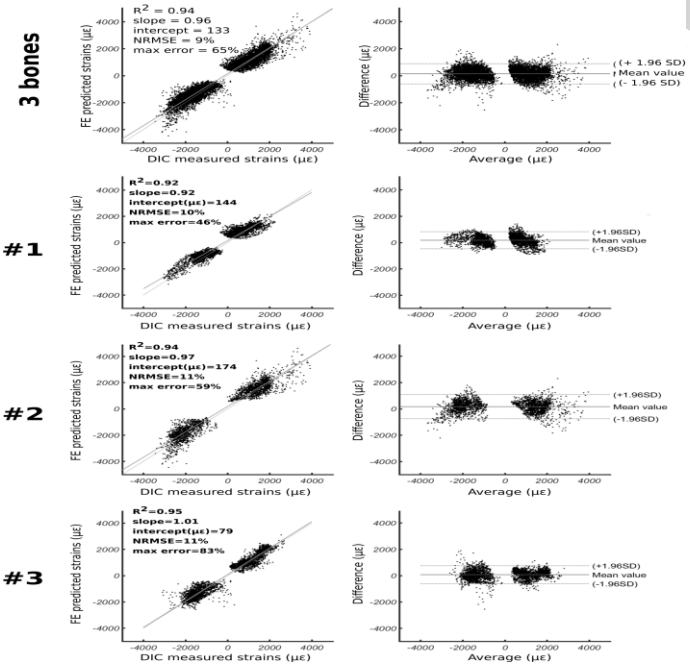

fig 3

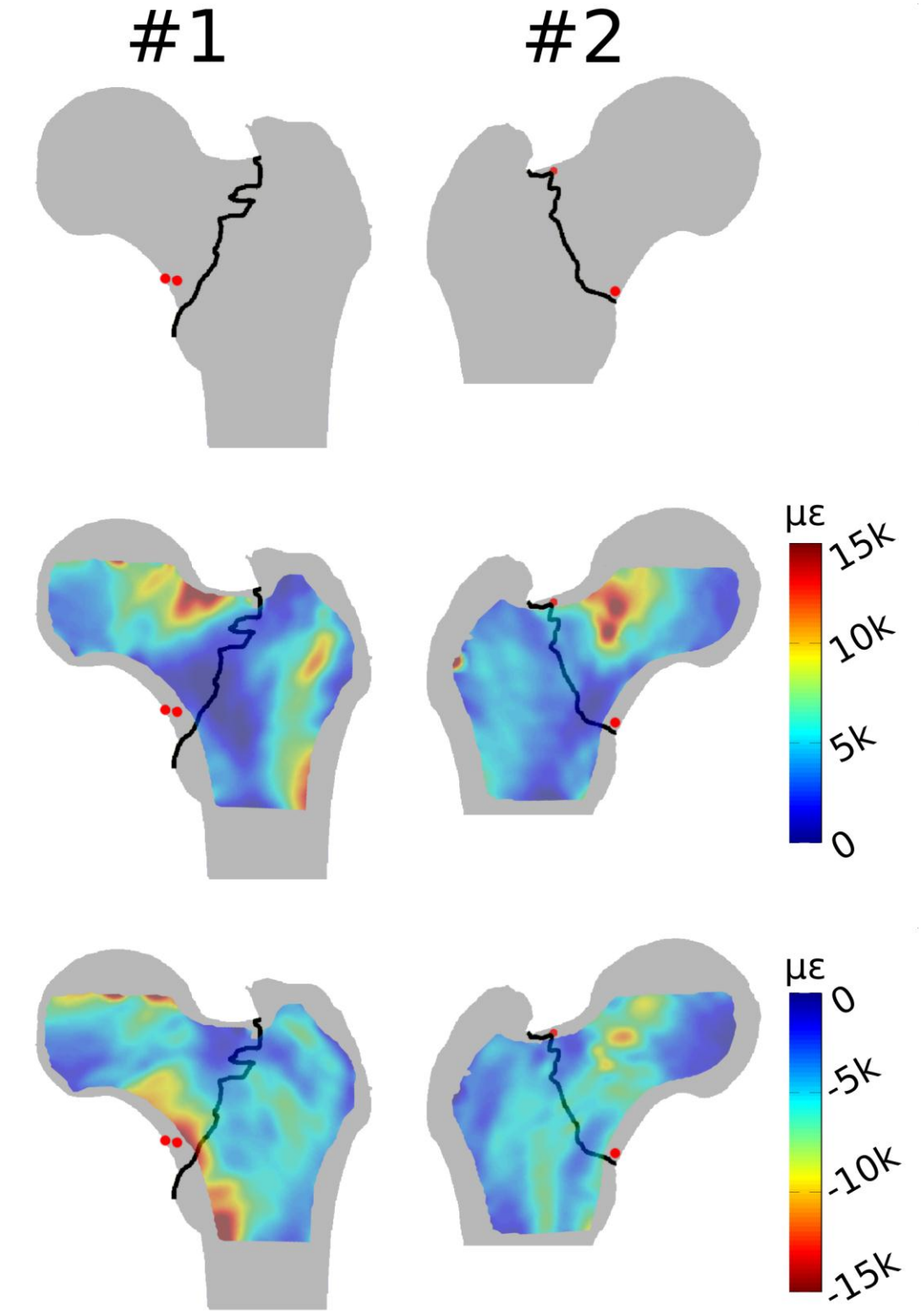

fig 4